

# CRITERIA FOR THE OCCURRENCE OF CROSSINGS BETWEEN THE ANGULAR DISTRIBUTIONS OF ELECTRON NEUTRINOS AND ANTINEUTRINOS IN THE SUPERNOVA CORE

SHASHANK SHALGAR<sup>1</sup> AND IRENE TAMBORRA<sup>1</sup>

<sup>1</sup> Niels Bohr International Academy and DARK, Niels Bohr Institute, University of Copenhagen, Blegdamsvej 17, 2100, Copenhagen, Denmark

*Draft version April 17, 2019*

## ABSTRACT

Neutrino fast pairwise conversions have been postulated to occur in the dense core of a core-collapse supernova (SN), possibly having dramatic consequences on the SN mechanism and the observable neutrino signal. One crucial condition favoring pairwise conversions is the presence of crossings between the electron neutrino and antineutrino angular distributions (i.e., electron neutrino lepton number crossings, ELN crossings). A stationary and spherically symmetric SN toy-model is constructed to reproduce the development of the neutrino angular distributions in the dense SN core in the absence of perturbations induced by hydrodynamical instabilities. By iteratively solving the neutrino Boltzmann equations including the collisional term, our model predicts that ELN crossings can develop only in the proximity of the decoupling region and for a shallow radial evolution of the baryon density, when the electron neutrino and antineutrino number densities are comparable. Such conditions are likely to occur only in the late SN stages. Interestingly, flavor instabilities induced by spatial or temporal perturbations are unlikely to generate ELN crossings dynamically.

*Keywords:* supernovae: general — neutrinos

## 1. INTRODUCTION

Core collapse supernovae (SNe) are among the densest sources in neutrinos (Mirizzi et al. 2016; Janka 2012). According to our current understanding, neutrinos are emitted as matter accretes on the proto-neutron star; they transport energy to finally revive the stalled shock-wave and power the SN explosion (Janka 2017). However, a detailed picture of the role of neutrinos remains unclear.

Understanding the impact of neutrino flavor conversions on the SN inner working is one of the crucial unsolved problems. In fact, neutrino flavor conversions have been traditionally neglected in SN transport, since they were expected to occur at radii larger than the shock radius and assumed to have a negligible impact on the shock revival, see e.g. Dasgupta et al. (2012).

Recent work suggests that the large density of neutrinos in the proximity of the neutrino decoupling region may favor the development of pairwise conversions (Sawyer 2016, 2009; Izaguirre et al. 2017). Contrary to our intuition, neutrino pairwise conversions could occur even in the absence of a hierarchy among the neutrino mass eigenstates and are independent on the neutrino energy; however, fast pairwise conversions crucially depend on the exact shape of the neutrino angular distributions and on the local neutrino density. The scale ruling such phenomenon is determined by  $(G_F |n_{\nu_e} - n_{\bar{\nu}_e}|)^{-1} \simeq \mathcal{O}(10)$  cm, with  $G_F$  being the Fermi constant and  $n_{\nu_e(\bar{\nu}_e)}$  the local (anti)neutrino number density. As a direct consequence of the “fast” interaction rate, neutrino pairwise conversions could possibly lead to flavor decoherence (Abbar & Volpe 2019; Dasgupta et al. 2017; Capozzi et al. 2019; Richers et al. 2019), affecting the neutrino heating within the gain radius as well as the SN nucleosynthesis, and the neutrino signal observable at Earth.

The criteria leading to the development of fast pairwise conversions were investigated in Refs. (Izaguirre et al. 2017; Capozzi et al. 2018, 2017). A non-negligible flux of neutrinos streaming backwards towards the proto-neutron star core as well as the presence of a crossing between the angular

distributions of electron neutrinos and antineutrinos (hereafter dubbed electron neutrino lepton number crossings, ELN crossing) have been pinpointed as crucial ingredients to trigger fast instabilities in the neutrino flavor space.

While ELN crossings are bound to occur in the case of compact binary mergers because of the particular merger geometry and the natural overall excess of electron antineutrinos with respect to electron neutrinos (Wu & Tamborra 2017; Wu et al. 2017), the situation seems to be more complex in the SN context. In fact, self-consistent spherically symmetric SN simulations in 1D did not find any evidence for ELN crossings over a range of progenitor masses (Tamborra et al. 2017). On the other hand, multi-D hydrodynamical simulations have reported mixed results (Abbar et al. 2018; Azari et al. 2019) depending on the different degree of approximation adopted in the implementation of the neutrino transport. In particular, the occurrence of LESA, the lepton-emission self-sustained asymmetry (Tamborra et al. 2014a,b) has been recently confirmed by a larger set of independent simulations (Janka et al. 2016; Walk et al. 2019; Vartanyan et al. 2019; O’Connor & Couch 2018; Glas et al. 2018). LESA has been also invoked as a possible ingredient favoring the development of the ELN crossings, see e.g. Izaguirre et al. (2017); Dasgupta et al. (2017).

The recent developments described above hint towards the need of a full implementation of the neutrino quantum kinetic equations, including collisions and flavor conversions (Volpe et al. 2013; Stirner et al. 2018; Sigl & Raffelt 1993; Vlasenko et al. 2014; Blaschke & Cirigliano 2016; Cirigliano et al. 2017). However, given the major numerical complications involved in the problem, this has not been tackled numerically in a self-consistent manner yet; see Richers et al. (2019) for a recent simplified attempt in this direction.

Hydrodynamical simulations of the core collapse do not include the physics of neutrino flavor conversions. Despite that, the simulations tracking the evolution of the neutrino angular distributions, see e.g. Refs. (Tamborra et al. 2017; Sumiyoshi et al. 2015; Nagakura et al. 2018), are extremely expensive in terms of computational resources. As a consequence, it

is challenging to explore the conditions leading to the development of ELN crossings and to track to the behavior of the neutrino angular distributions in the later stages of the core collapse.

In this work, by assuming spherical symmetry and that a stationary solution is reached, we develop a simplified model to mimic the SN core microphysics and iteratively solve the neutrino Boltzmann equations with the inclusion of the collisional term. Our goal is to estimate the neutrino angular distributions of  $\nu_e$  and  $\bar{\nu}_e$  in the neutrino trapping region and follow their evolution until neutrinos are fully decoupled in the different SN phases. By neglecting complications coming from the SN hydrodynamics, we aim at identifying the microphysical ingredients leading to the development of ELN crossings and discuss their implications for the physics of flavor conversions.

The outline of the paper is as follows. In Sec. 2, we present our stationary and spherically symmetric SN model and the iterative method employed to solve the neutrino Boltzmann equations by taking into account the collision term. In Sec. 3, we investigate the occurrence of ELN crossings by introducing a simple evaluation criterion; we first test the latter for a simplified scenario and then discuss its implications through a more realistic framework based on inputs from a 1D hydrodynamical SN model. Section 4 focuses on exploring whether ELN crossings can be generated dynamically by the occurrence of neutrino flavor conversions because of spatial or temporal perturbations. A discussion on our findings and conclusions are reported in Sec. 5.

## 2. NEUTRINO EQUATIONS OF MOTION IN THE DENSE PROTO-NEUTRON STAR

In this Section, we first introduce the neutrino kinetic equations and then describe the method employed to solve them in spherical symmetry and derive the neutrino angular distributions.

### 2.1. Neutrino Kinetic Equations

In the interior of a SN, the neutrino number density as well as the baryon density are very large and neither neutrino-neutrino self-interactions (coherent forward scattering) nor neutrino-matter scatterings (incoherent scattering) can be ignored. The coherent and incoherent parts of the neutrino evolution can have a significant feedback on each other. In fact, the neutrino-matter cross-section is flavor dependent, while the non-linear neutrino flavor evolution depends on the spatial distribution of neutrinos, which is determined by the neutrino matter scattering cross-section. However, the interplay between the non-linearity arising from the neutrino self-interaction and scatterings with the nuclear matter remains enigmatic.

Throughout this paper, for the sake of simplicity, we assume that  $(\nu_e, \nu_x)$  describes the neutrino flavor basis with  $\nu_x$  being a mixture between  $\nu_\mu$  and  $\nu_\tau$  and similarly for antineutrinos. The equation of motion describing the neutrino flavor evolution, including coherent and incoherent components, can be conveniently expressed in terms of a  $2 \times 2$  density matrix,  $\rho$  (and  $\bar{\rho}$  for antineutrinos).

The neutrino kinetic equation, for each neutrino momentum mode  $\vec{p}$ , is given by

$$i \frac{\partial \rho(\vec{x}, \vec{p}, t)}{\partial t} + \vec{v} \cdot \nabla \rho(\vec{x}, \vec{p}, t) + \vec{F} \cdot \nabla_p \rho(\vec{x}, \vec{p}, t) = [H, \rho(\vec{x}, \vec{p}, t)] + iC[\rho(\vec{x}, \vec{p}, t)], \quad (1)$$

where  $\vec{x}$  and  $t$  describe the spatial and temporal coordinates, and  $\vec{v}$  is the neutrino velocity. The Hamiltonian  $H$  contains three components, a term embedding the neutrino mixing in vacuum, a term describing the interactions of neutrinos with the SN matter background, and a term describing the neutrino-neutrino interactions, see e.g. Mirizzi et al. (2016). Since we are interested in exploring the development of the ELN crossings, we will neglect neutrino flavor conversions in the following, unless otherwise stated.

The  $C[\rho]$  describes the scattering of neutrinos with the medium. While  $\vec{F} \cdot \nabla_p \rho$  tracks the effect of external forces on the neutrino field; we will assume that the latter has a negligible contribution in the following. Hereafter we will also use  $\hbar = c = 1$ .

The density matrix is normalized such that the terms on the diagonal give the total number density of neutrinos for fixed  $(\vec{r}, t)$ . Notably, deep in the SN core the electron (anti-)neutrinos are highly degenerate and are in thermal equilibrium with the SN medium. Therefore, the (anti-)neutrino number densities are well described by a Fermi-Dirac distribution:

$$\frac{dn_\nu}{dE} = \frac{1}{2\pi^2} \frac{E^2}{e^{(E-\mu_\nu)/T} + 1}, \quad (2)$$

where the  $\mu_\nu$  is the neutrino chemical potential, such that  $\mu_{\nu_e} = -\mu_{\bar{\nu}_e}$  and  $\mu_{\nu_x} = \mu_{\bar{\nu}_x} = 0$ , and  $T$  is the temperature of the SN matter. The off-diagonal terms of the density matrix, instead, are related to the probability of having a flavor transition.

Solving Eq. 1 may not appear to be a daunting task at first glance. However, it should be noted that the collision term  $C[\rho]$  (and  $\bar{C}[\bar{\rho}]$ ) entails a six dimensional integral for each  $(\vec{x}, \vec{p}, t)$ . The partial differential equation cannot be solved using standard discretization techniques in a 7D space due to the limitations of available computational power. Imposing symmetries on the system is not easy due to spontaneous breaking of symmetries in momentum and real space (Mirizzi et al. 2016).

The left-hand-side of the Eq. 1 contains the convective term, which can be reduced to  $[\cos \theta \partial \rho(\vec{x}, \vec{p}, t) / \partial r]$  under the assumption of spherical symmetry and stationarity. It should be noted that, due to the non-linearity of the neutrino-neutrino term, the convective term may lead to spontaneous breaking of spherical symmetry (Raffelt et al. 2013; Duan & Shalgar 2015). For the sake of simplicity, in the following, we will assume that spherical symmetry is preserved and ignore the convective term.

The exact shape of the neutrino angular distributions in the SN core depends on the interactions described by the collision term. The collision term,  $C[\rho]$ , contains two components: the loss and gain terms. The loss term accounts for the reduction of the neutrino number flux for a given direction and momentum due to scattering to another direction and momentum; the gain term, instead, accounts for scattering of neutrinos into a given direction and momentum state.

It should be noted that the equations of motion discussed in this Section do not fall in the category of initial value problem. In the following Section, we outline the technique we use to tackle this problem numerically.

### 2.2. Stationary and Spherically Symmetric Supernova Model

Collisions of neutrinos with matter determine the spatial distribution of neutrinos in the SN interior. However, there is a feedback between the flavor dependent neutrino cross-section and the neutrino flavor evolution. As we will see in the fol-

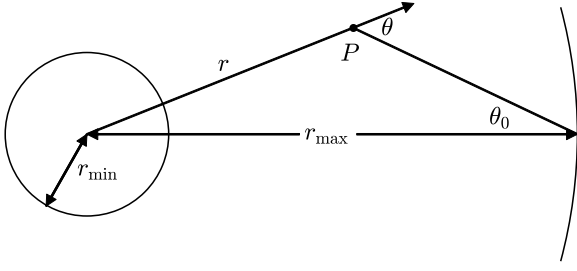


**Figure 1.** Schematic representation of the stationary and spherically symmetric SN model. The boundary conditions are set at the innermost radius  $r_{\min}$  and at the outermost radius  $r_{\max}$ . Each point  $P$  is characterized by a global set of coordinates  $(r, \theta_0)$  with  $\theta_0$  defined with respect to the outermost spherical surface. For each point  $P$ , we also introduce a local system of coordinates through the angle  $\theta$ . The angles  $\theta$  and  $\theta_0$  are related through Eq. 4.

lowing, the radial profile of the baryon density strongly affects the development of ELN crossings because of the neutrino-matter interactions. To first order, we can ignore the flavor evolution of the neutrinos and focus on scatterings to investigate the conditions under which ELN crossings develop. We make the following assumptions:

1. The number density of neutrinos is locally conserved.
2. Each scattering is locally isotropic.
3. Energy-averaged, flavor-dependent neutrino distributions are adopted.
4. Only two neutrino flavor eigenstates are considered.

As discussed in the previous Section, Eq. 1 requires to define boundary conditions instead of initial conditions. In order to obtain a stationary solution in the presence of collisions, we adopt an iterative method. Note that we assume that our model does not depend on  $t$  and the azimuthal angle  $\phi$ .

Our spherically symmetric model is sketched in Fig. 1. We assume that neutrinos are radiated by an inner surface of radius  $r_{\min}$  and propagate until they reach an outermost surface of radius  $r_{\max}$ . Each point  $P$  in the SN sphere is characterized by the radius  $r$  and the angle  $\theta_0$ , where  $\theta_0$  has been defined with respect to the outermost surface. For each  $P$ , we further introduce a set of coordinates  $\theta$  to characterize the local angular distribution of neutrinos. Moreover, given that the energy-dependent quantities entering the neutrino equation of motion are averaged over the neutrino energy distribution, we will effectively solve Boltzmann equations depending on the neutrino scattering angle, but not on their momentum.

In the first step of our iteration method, we ignore the backward flux of neutrinos (i.e., assume a null neutrino flux for  $\cos \theta < 1$ ) and evolve the following equation of motion

$$\cos \theta_i \frac{d\rho(r)_i^\uparrow}{dr} = \sum_j (-C^{\text{loss}} \rho(r)_i^\uparrow + C^{\text{gain}} \rho_j^\uparrow(r)) \Delta \cos \theta_j \quad (3)$$

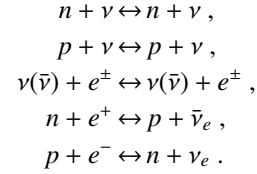
where the subscripts  $(i, j)$  denote the indexes of the angular bins.  $\Delta \cos \theta_j$  is the width of the  $j^{\text{th}}$  angular bin, which depends on the radius and has to be calculated at each radial step, as we will see in the following.

Equation 3 is solved from  $r_{\min}$ , arbitrarily set to 5 km, up to  $r_{\max}$ , fixed at 60 km. Note that the choice of  $r_{\min}$  guarantees that the collisional rate is large enough to re-distribute

the neutrinos in  $\theta$  homogeneously, while  $r_{\max}$  has been fixed outside of the neutrino trapping region and is large enough to not affect the neutrino angular distributions at decoupling. During the first iteration, the resulting flux of  $(e, x)$  neutrinos and antineutrinos in the forward direction is stored at regular radial intervals.

In order to locally conserve the neutrino number densities, we set the loss coefficient,  $C^{\text{loss}}$ , equal to the gain coefficient,  $C^{\text{gain}}$ . The loss and gain coefficients are proportional to the product of the number density of scatterers and the cross-section for each interaction channel averaged over the neutrino energy distribution, i.e.  $C^{\text{loss}}, C^{\text{gain}} \propto n_{\text{targets}} \langle F \sigma \rangle$ , with  $F$  being the Pauli blocking factor, and  $\langle \sigma \rangle$  the cross section averaged over the neutrino energy distribution.

The cross-sections entering  $C^{\text{loss}}$  and  $C^{\text{gain}}$  have been calculated for the following reactions:



Each cross-section has been implemented as prescribed in Bowers & Wilson (1982). We also employed flavor-dependent neutrino distributions defined along the lines of Eq. 2, and the respective mass-dependent Fermi-Dirac distributions have been adopted for the nucleons. In particular, the local density of nucleons has been defined through the baryon density  $\rho_B$  and the electron fraction  $Y_e$  [ $n_n \simeq \rho_B(1 - Y_e)$  for neutrons and  $n_p \simeq \rho_B Y_e$  for protons]. For each reaction, the Pauli blocking factor  $F$  has been computed following Refs. (Raffelt 1996; Bruenn 1985) and included in the collision term. Note that, although neutrinos and antineutrinos undergo the same kind of neutral current interactions, a small difference appears in their cross sections. As we will discuss afterwards, this will also factor in in the eventual development of ELN crossings.

The first term on the right hand side of Eq. 3 is the loss term that depends on the number of neutrinos in the  $i^{\text{th}}$  bin and on the phase space. However, we perform the integration numerically to ensure that the numerical error arising from the discretization of the gain term is canceled by that of the loss term. The  $\cos \theta$ -term on the left hand side of Eq. 3 takes into account the dependence of the path length on the zenith angle.

We bin the neutrino trajectories with respect to the global angle defined at  $r_{\max}$  denoted by  $\theta_0$ . In particular, in the numerical runs, the angular grid has been chosen to be uniform in  $\cos^2 \theta_0$ . For all the results presented in this paper we used 200 angular bins in the global coordinate system. As the ratio  $r_{\max}/r_{\min}$  increases, finer angular resolution is required to ensure there is a sufficient number of angular bins that intersect the  $r_{\min}$  sphere.

The angle in the global coordinate system  $\theta_0$  is related to the local angle  $\theta$  by the following relation,

$$\cos \theta = \sqrt{1 - \left(\frac{r_{\max}}{r}\right)^2 (1 - \cos^2 \theta_0)}. \quad (4)$$

For fixed  $P$ , if  $\text{Im}(\cos \theta) \neq 0$ , then the neutrino trajectory is discarded.

After the completion of this first step of our iteration

method, we evolve the equations of motion for the backward flux from  $r_{\max}$  to  $r_{\min}$

$$\cos \theta_i \frac{d\rho(r)_i^\downarrow}{dr} = \sum_{j,j'} \left( -C^{\text{loss}} \rho(r)_i^\downarrow + C^{\text{gain}} \rho_j^\downarrow(r) + C^{\text{gain}} \rho_j^{\text{pr}\uparrow}(r) \right) \Delta \cos \theta_j. \quad (5)$$

Here, the superscript ‘pr’ is used to denote that the values for the components of the density matrix are interpolated using the solutions of Eq. 3. The width of the angular bins is the same for forward and backward going neutrinos ( $\Delta \cos \theta_j = \Delta \cos \theta_j'$ ). Notably, during this iteration, the gain term in the equation of motion receives a contribution from the forward flux stored during the previous iteration.

Upon completion of the first iteration (forward and backward), we obtain the initial conditions of the equations of motion for the next iteration round. Since  $r_{\min}$  is chosen to be in a region of extremely large matter density, the angular distribution is essentially uniform and we can set the forward flux at  $r_{\min}$  equal to the backward flux for all angular bins. After each backward iteration, we rescale the normalization of the backward flux by an amount that is proportional to the flux at  $r_{\min}$  to compensate for the loss of neutrinos by diffusion at  $r_{\max}$ , and achieve a steady state solution. The relative normalization between  $\nu_e$  and  $\bar{\nu}_e$  is thus determined by the dynamics of collisions in our model. This is a crucial aspect, as the occurrence of ELN crossings (or lack thereof) is determined in large part by the relative normalization of the  $\nu_e$  and  $\bar{\nu}_e$  angular distributions.

Using the initial conditions obtained by the former backward iteration, the equations of motion are then evolved in the forward direction, while using the interpolated values from the solution of Eq. 5:

$$\cos \theta_i \frac{d\rho(r)_i^\uparrow}{dr} = \left( -C^{\text{loss}} \rho(r)_i^\uparrow + \sum_j C^{\text{gain}} \rho_j^\uparrow(r) + \sum_{j'} C^{\text{gain}} \rho_j^{\text{pr}\downarrow}(r) \right) \Delta \cos \theta_j. \quad (6)$$

We repeatedly solve Eqs. 5 and 6 for neutrinos and antineutrinos using interpolated values for the components of the density matrix that have the superscript ‘pr’. We find that around 15 iterations are sufficient to achieve numerical convergence of the results. Notably, this procedure guarantees that the steady state solution is independent on the initial conditions used in the first iteration and determined by self-consistency alone.

In order to be certain that our simple SN model reproduces flavor-dependent neutrino angular distributions in agreement with the literature, we adopted the inputs of the SN models employed in Ref. (Tamborra et al. 2017) and computed the expected angular distributions. Our results are in agreement with the ones presented in Tamborra et al. (2017).

Figure 2 shows an illustrative example of the resultant  $\nu_e$  angular distribution in arbitrary units. The angular distribution has been plotted at different radii and has been obtained by using the inputs from a 1D hydrodynamical model of a  $18.6 M_\odot$  SN with SFHo nuclear equation of state (Garching Supernova Archive) for  $t_{\text{p.b.}} = 0.25$  s, which we will use in Sec. 3.2. One can see that the neutrino angular distribution is almost isotropic in  $\cos \theta$  when neutrinos are trapped and be-

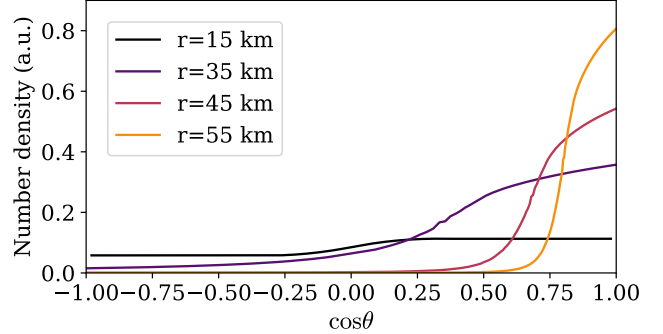


**Figure 2.** Illustrative example of the  $\nu_e$  angular distribution as a function of  $\cos \theta$  in arbitrary units and for different radii ( $r$ ) before and after decoupling. The neutrino angular distribution is almost isotropic in  $\cos \theta$  in the trapping regime in the SN core; as  $r$  increases and neutrinos approach the free-streaming regime, the neutrino angular distribution becomes forward peaked.

comes forward peaked as neutrinos approach the free streaming regime. In particular, the  $\nu_e$  angular distribution becomes more peaked than the  $\bar{\nu}_e$  as expected by the different interaction rates of electron neutrinos and antineutrinos. We refer the reader to Refs. (Tamborra et al. 2017; Ott et al. 2008; Sarikas et al. 2012) for more details on the radial evolution of the flavor-dependent neutrino angular distributions.

### 3. CRITERIA FOR THE APPEARANCE OF CROSSINGS IN THE ELECTRON NEUTRINO LEPTON NUMBER DISTRIBUTION

In this Section, we explore the microphysical conditions leading to the occurrence of ELN crossings. We first focus on a simple toy model in order to pinpoint the main ingredients favoring the development of ELN crossings and present a criterion to predict the crossing occurrence in the absence of SN hydrodynamical instabilities. The development of ELN crossings in a more realistic SN setup is then investigated by employing inputs from a 1D hydrodynamical simulation of the core collapse.

#### 3.1. Toy-model example

In order to explore what are the conditions leading to the occurrence of ELN crossings, we perform simulations by employing the iterative method described in Sec. 2.2. For simplicity, in this Section, we assume a constant matter temperature  $T$ , and a constant chemical potential for both neutrinos and matter; all set to 10 MeV. In order to characterize the neutrino interaction strength, the total energy-averaged neutrino and antineutrino mean free path is defined as

$$\lambda_{\nu_e, \bar{\nu}_e}^{-1} \approx \sum_l \left( \frac{1}{\langle \sigma n_{\text{targets}} \rangle_l} \right)^{-1}, \quad (7)$$

where  $l$  denotes the various neutrino-matter reaction channels listed in Sec. 2.2; the neutrino number densities and cross-sections have been modelled as described in Sec. 2.2. One can easily show that the dominant interaction rates setting the difference between the  $\nu_e$  and  $\bar{\nu}_e$  angular distributions, eventually leading to ELN crossings, are the charged current interactions with a subleading contribution coming from the neutral current interactions. Hence,  $\lambda_{\nu_e}/\lambda_{\bar{\nu}_e}$  and the resultant local number density of  $\nu_e$  and  $\bar{\nu}_e$  are the crucial quantities in setting the relative ratio between the angular distributions of  $\nu_e$  and  $\bar{\nu}_e$ . In our toy-model, we assume  $\lambda_{\nu_e}/\lambda_{\bar{\nu}_e} \approx 0.3$ .

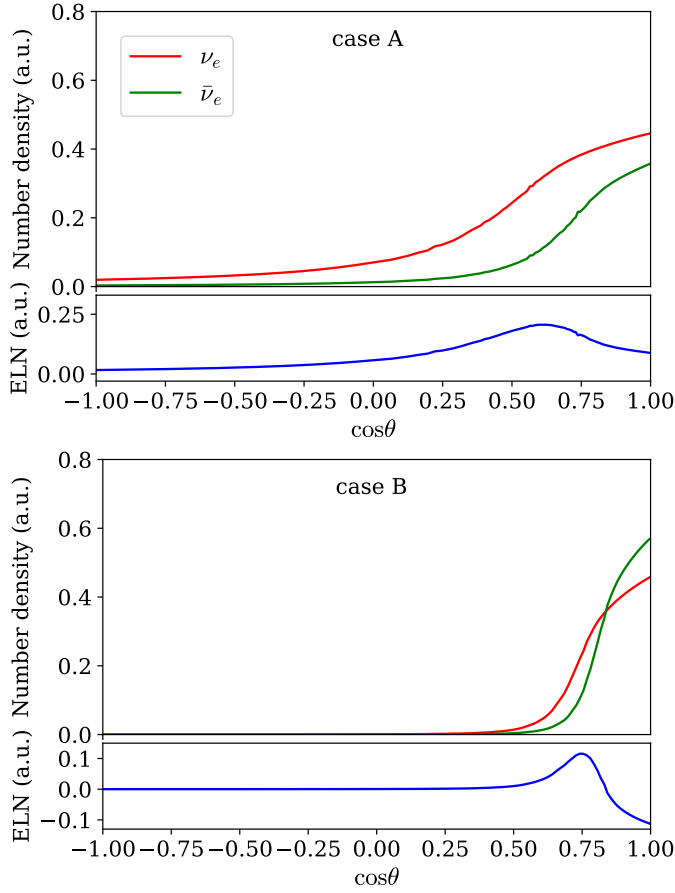


**Figure 3.** *Top:* Angular distributions for toy model “case A” (see text for details) for  $\nu_e$  in red and  $\bar{\nu}_e$  in green as a function of  $\cos\theta$  in arbitrary units. The angular distributions have been extracted after neutrino decoupling. The shallow baryon density profile ensures that the decoupling radius of  $\nu_e$  is significantly larger than the one of  $\bar{\nu}_e$  given the difference in their interaction strength. *Bottom:* Angular distributions for toy model “case B.” The rapidly falling baryon density profile implies the close vicinity of the neutrino decoupling radii and the formation of the ELN crossing. The bottom panels for “case A” and “case B” show the ELN distribution as a function of  $\cos\theta$ .

We assume a baryon density profile that falls exponentially with respect to the radius and distinguish between two cases. A first case involves a shallow baryon density profile (“case A”),

$$\rho_{B,\text{caseA}}(r) = 10^{14} \exp(0.25(5 - r)) \text{ gm/cc}, \quad (8)$$

and a second case that includes a steeply falling baryon density profile (“case B”)

$$\rho_{B,\text{caseB}}(r) = 10^{14} \exp(0.5(5 - r)) \text{ gm/cc}; \quad (9)$$

Figure 3 show the stationary solution obtained for the  $\nu_e$  (in red) and  $\bar{\nu}_e$  (in green) angular distributions as a function of  $\cos\theta$  for “case A” on the top and for “case B” on the bottom in arbitrary units. Note that the angular distributions of  $\nu_x$  and their antineutrinos are also computed, but we do not show them here for simplicity. The plotted angular distributions have been extracted at  $r \approx 40$  km and  $r \approx 30$  km, respectively; i.e., after the neutrino decoupling. One can see that while “case A” does not lead to the formation of an ELN crossing, “case B” does. For completeness, the bottom panels of “case A” and “case B” in Fig. 3 show the resultant ELN distribution ( $\nu_e - \bar{\nu}_e$ ) in arbitrary units and as a function of  $\cos\theta$ .

Figure 4 shows the radial evolution of  $\text{ELN}(\cos\theta = 1)$  for “case A” (in violet) and “case B” (in blue). For each case, the

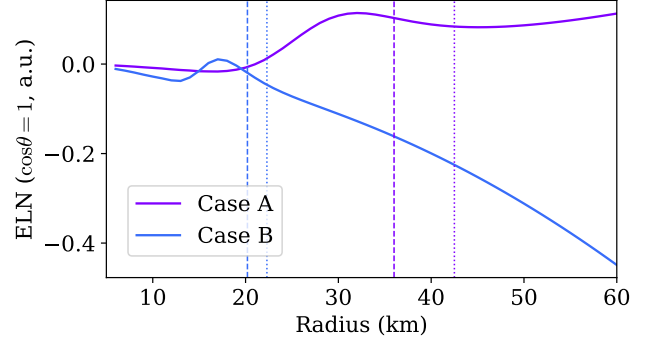


**Figure 4.** Radial evolution of the  $\text{ELN}(\cos\theta = 1)$  for toy model “case A” in violet and “case B” in blue. The radius of onset of free streaming is marked by two vertical lines for each case to guide the eye; the dashed line is for  $\nu_e$  and the dotted one for  $\bar{\nu}_e$ . Neutrinos and antineutrinos decouple at smaller radii for “case B” and the onset of free streaming radius of  $\nu_e$  is closer to the one of  $\bar{\nu}_e$  for “case B” than for “case A.”

**Table 1**

Ratio of the electron neutrino and antineutrino number densities ( $n_{\nu_e}/n_{\bar{\nu}_e}$ ) at the radius of the onset of free streaming of  $\nu_e$  for “case A” and “case B,” see text for details.

	$n_{\nu_e}/n_{\bar{\nu}_e}$
case A	2.11
case B	1.24

onset of the free-streaming regime of  $\nu_e$  and  $\bar{\nu}_e$  is marked by two vertical lines to guide the eye; since we only need an approximate estimation of the region where the neutrinos start to stream freely and are fully decoupled from matter, we define the radius of onset for the free-streaming regime as the radius where the forward flux ( $\cos\theta > 0$ ) is 10 times larger than the backward flux ( $\cos\theta < 0$ ). One can see that the free-streaming regime is reached at larger  $r$  for “case A.” Moreover, the onset radius of free-streaming for  $\nu_e$  is always smaller than the one of  $\bar{\nu}_e$  given the difference in the interaction strengths. The two radii are separated by a larger distance in “case A.”

By looking at Figs. 3 and 4, one can see that ELN crossings originate in the proximity of the neutrino free-streaming region in “case B.” Moreover, because of the different baryon profiles employed in “case A” and “case B,” the decoupling regions of  $\nu_e$  and  $\bar{\nu}_e$  occur in very different spatial regions for “case A” while they are close to each other for “case B.” This implies that the  $\nu_e$  and  $\bar{\nu}_e$  angular distributions are more similar to each other in the proximity of the decoupling region in “case B” than in “case A.” This is also proved by the fact that the total local number densities of  $\nu_e$  and  $\bar{\nu}_e$  are more similar to each other in the proximity of the decoupling region in “case B,” as shown in Table 1.

This toy-model example shows that ELN crossings can develop only in the proximity of the neutrino decoupling region. Moreover, the decoupling of  $\nu_e$  should occur in a radial region close to where the one of  $\bar{\nu}_e$  happens and their local number densities should be comparable. If those conditions are fulfilled, ELN crossings are likely to develop.

### 3.2. Supernova model example

We now extend our findings to a more complex case involving the radial dependence of the main SN quantities. We base our estimations on the inputs from a 1D hydrodynamical model of a  $18.6 M_\odot$  SN with SFHo nuclear equation

**Table 2**

Ratio of the electron neutrino and antineutrino number densities ( $n_{\nu_e}/n_{\bar{\nu}_e}$ ) at the radius of the onset of free streaming of  $\nu_e$  for three different post-bounce times  $t_{p.b.} = 0.25, 0.5$  and  $1$  s of our benchmark SN model.

	$n_{\nu_e}/n_{\bar{\nu}_e}$
$t_{p.b.} = 0.25$ s	1.31
$t_{p.b.} = 0.5$ s	0.96
$t_{p.b.} = 1$ s	1.08

of state and gravitational mass of  $1.4 M_{\odot}$  (Garching Supernova Archive) that we adopt as benchmark case, and select post-bounce time snapshots representative of the different SN phases. Note that the hydrodynamical simulation does not provide the neutrino angular distributions that are instead estimated iteratively through our stationary and spherically symmetric model.

The top panel of Fig. 5 shows the baryon density as a function of the radius for three different post-bounce times  $t_{p.b.} = 0.25, 0.5$  and  $1$  s, in violet, blue and cyan respectively. The radii of the onset of free-streaming of  $\nu_e$  and  $\bar{\nu}_e$  are marked through the vertical lines to guide the eye. One can see that, as  $t_{p.b.}$  increases, neutrinos start to free-stream at smaller radii, closer to the SN core. Moreover, as time progresses, the baryon density profile becomes steeper in the proximity of the region of onset of free streaming. Another interesting aspect is that, for fixed  $t_{p.b.}$ , the free-streaming radii of  $\nu_e$  and  $\bar{\nu}_e$  differ from each other at earlier post-bounce times and become similar to each other at later times. For earlier times, the electron fraction  $Y_e$  is larger at radii smaller than the free-streaming one as shown in the middle panel of Fig. 5. The bottom panel of Fig. 5 shows the ratio of the mean free paths  $\lambda_{\nu_e}/\lambda_{\bar{\nu}_e}$  as a function of the radius; in the proximity of the free-streaming radius,  $\lambda_{\nu_e}/\lambda_{\bar{\nu}_e} \leq 1$ . The ratio between the  $\nu_e$  and  $\bar{\nu}_e$  number densities at the radius of onset of free streaming is reported in Table 2 for the three studied  $t_{p.b.}$ . One can see that  $n_{\nu_e}/n_{\bar{\nu}_e} \rightarrow 1$  as  $t_{p.b.}$  increases.

Figure 6 shows the resultant angular distributions in arbitrary units for  $\nu_e$  and  $\bar{\nu}_e$  as a function of  $\cos\theta$  for  $t_{p.b.} = 0.25, 0.5$  and  $1$  s from top to bottom, respectively. Those angular distributions have been obtained with our iterative method by employing the SN inputs shown in Fig. 5, together with the radial profiles of the chemical potentials for neutrinos and nucleons and the medium temperature extracted from the hydrodynamical simulation. We plot the angular distributions at an arbitrary radius of  $40$  km, i.e. after the neutrino decoupling occurred. For  $t_{p.b.} = 0.25$  s, no ELN crossing is found as the number density of  $\nu_e$  remains larger than the one of  $\bar{\nu}_e$  due to the shallow baryon density profile. At late times ( $t_{p.b.} \gtrsim 0.5$  s), the baryon density profile becomes steeper; as a result the free-streaming radii of  $\nu_e$  and  $\bar{\nu}_e$  become closer and the number densities of  $\nu_e$  and  $\bar{\nu}_e$  become comparable. Hence, ELN crossings are favored.

Figure 7 shows the radial evolution of ELN( $\cos\theta = 1$ ) for  $t_{p.b.} = 0.25, 0.5$  and  $1$  s. As discussed for the toy-model, ELN crossings only occur in the proximity of the neutrino free-streaming region.

In conclusion, our stationary and spherically symmetric SN model strongly suggests that ELN crossings can only occur within the spatial regions where neutrinos and antineutrinos decouple and start to free stream. Moreover, a steep drop of the baryon density profile, as typical of the late SN stages, together with comparable number densities of  $\nu_e$  and  $\bar{\nu}_e$  and  $\lambda_{\nu_e}/\lambda_{\bar{\nu}_e} \leq 1$  in the decoupling region, would favor the devel-

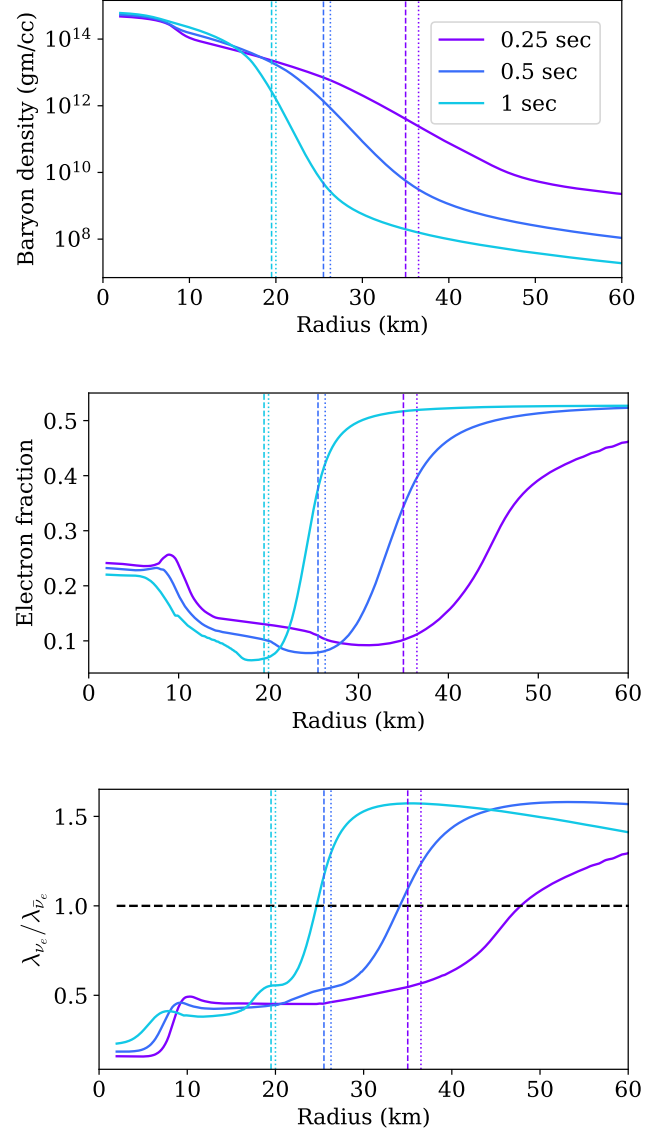


**Figure 5.** *Top:* Baryon density as a function of radius for  $t_{p.b.} = 0.25, 0.5$  and  $1$  s, in violet, blue and cyan respectively, for the  $18.6 M_{\odot}$  SN model adopted as benchmark case in this work. The radii of onset of free streaming are marked by two vertical lines, the dashed one is for  $\nu_e$  and the dotted one for  $\bar{\nu}_e$ , to guide the eye. In the region of decoupling the baryon density falls off much more rapidly as  $t_{p.b.}$  increases. *Middle:* Electron abundance as a function of radius for  $t_{p.b.} = 0.25, 0.5$  and  $1$  s.  $Y_e$  is smaller in the proximity of the decoupling radius for larger  $t_{p.b.}$ . *Bottom:* Ratio of mean free paths of  $\nu_e$  and  $\bar{\nu}_e$ . It should be noted that the mean free path of  $\bar{\nu}_e$  is larger than that of  $\nu_e$  before decoupling.

opment of angular distributions that are similar to each other; as a consequence, ELN crossings develop given the different interaction rates of  $\nu_e$  and  $\bar{\nu}_e$ . Our results confirm the findings of Refs. (Tamborra et al. 2017; Azari et al. 2019) where only the early SN stages were analyzed and no crossing was found. Note that, although we only show the results for three selected snapshots here, we have estimated the angular distributions for  $t_{p.b.} \in [0.25, 0.5]$  s and found that  $t_{p.b.} = 0.5$  s is the first snapshot for which the ELN crossing develops for the adopted SN model.

Our stationary and spherically symmetric SN model does not include any macroscopic asymmetry eventually induced by the hydrodynamical instabilities. The occurrence of the

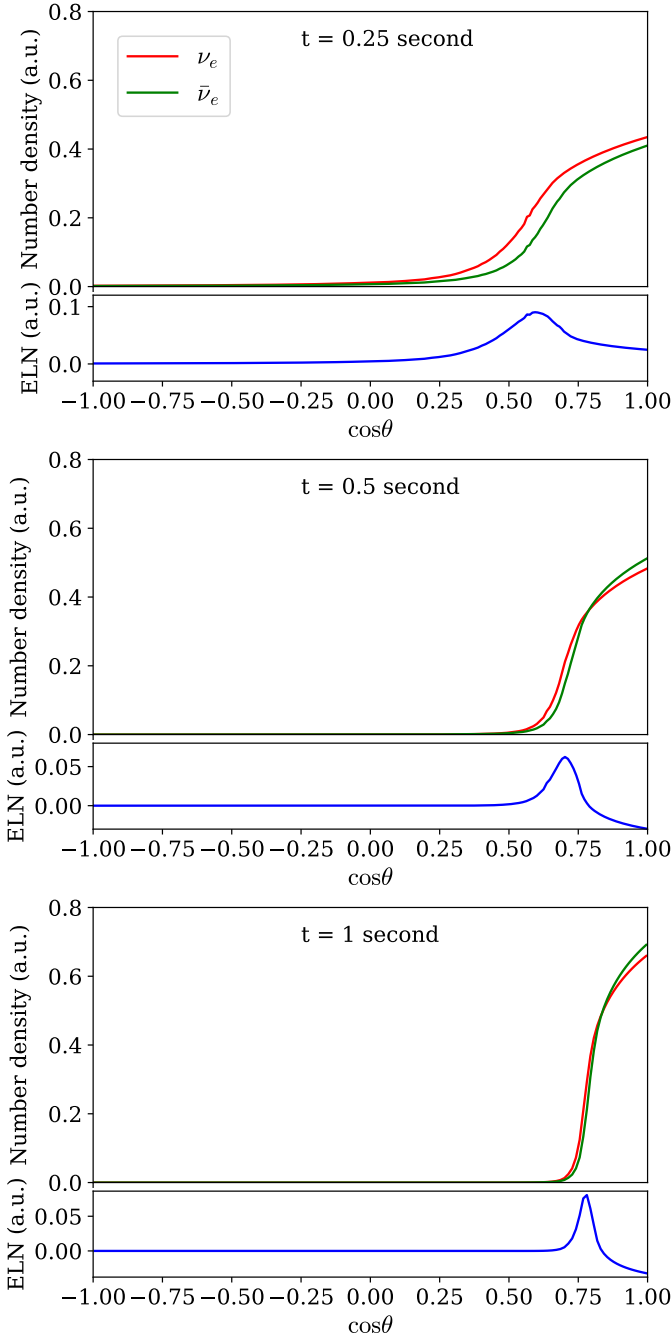


**Figure 6.** *Top:* Angular distributions of  $\nu_e$  in red and  $\bar{\nu}_e$  in green in arbitrary units, for  $t = 0.25$  s as a function of  $\cos \theta$  for our benchmark SN model. The angular distributions have been extracted at 40 km, i.e. after decoupling. The lower panel shows the angular distribution of the ELN. The excess in the total number of  $\nu_e$  prevents an ELN crossing. *Middle:* Angular distributions of  $\nu_e$  and  $\bar{\nu}_e$  for  $t = 0.5$  s. An ELN crossing occurs as the decoupling regions of  $\nu_e$  and  $\bar{\nu}_e$  become closer to each other and their number densities are comparable. *Bottom:* Angular distributions of  $\nu_e$  and  $\bar{\nu}_e$  for  $t = 1$  s. The ELN becomes negative in the forward direction implying that a crossing occurs.

LESA instability has been pinpointed as a possible favorable condition leading to ELN crossings (Izaguirre et al. 2017; Dasgupta et al. 2017). Our stationary SN model hints that, excluding the transition regions when the ELN changes sign in the presence of LESA, in the SN angular regions of net  $\bar{\nu}_e$  excess, the  $\bar{\nu}_e$  and  $\nu_e$  number densities would roughly “swap” and our criteria should still hold. Hence, we expect that, only if the LESA instability is sustained until the late SN phases,

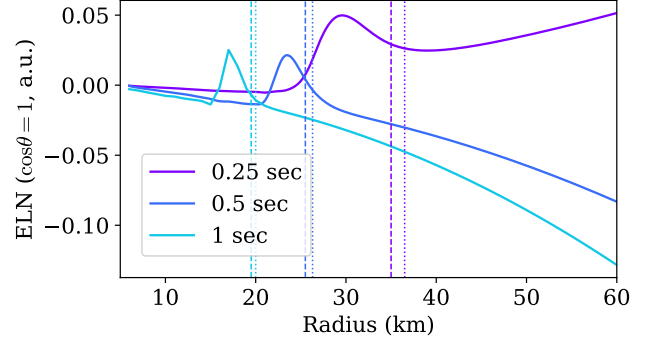


**Figure 7.** Radial evolution of  $\text{ELN}(\cos \theta = 1)$  as a function of the radius in arbitrary units, for  $t_{p,b.} = 0.25, 0.5$  and 1 s, in violet, blue, and cyan respectively. For  $t_{p,b.} = 0.5$  and 1 s, ELN crossings appear in the proximity of the neutrino free-streaming region, i.e.,  $\text{ELN}(\cos \theta = 1)$  changes sign.

then ELN crossings may develop, otherwise the  $\bar{\nu}_e$  excess should not be a sufficient condition for crossings to arise.

Our model cannot fully test the conditions leading to crossings in the presence of the LESA instability self-consistently, since this would require a break of the spherical symmetry. Therefore, our conjectures remain to be tested through self-consistent 3D hydrodynamical simulations and will be subject of further work.

#### 4. DYNAMICAL GENERATION OF CROSSINGS IN THE ELECTRON NEUTRINO LEPTON NUMBER DISTRIBUTION

The presence of ELN crossings, or lack thereof, is determined by the radial profile of  $\lambda_{\nu_e}/\lambda_{\bar{\nu}_e}$ , the baryon density profile, as well as  $n_{\nu_e}/n_{\bar{\nu}_e}$ , which is related to the former two, in the trapping region. However, as discussed in Sec. 3, the presence of ELN crossings is not only determined by the local conditions but it indirectly feels the effects of distant regions in the SN through collisions. If neutrino conversions occur in the SN core due to a local fluctuation triggering instabilities in the flavor space (independently from the existence of ELN crossings), then our analysis should be modified. In this Section, we analyze whether the existence of flavor conversions may impact the conditions leading to the development of ELN crossings and therefore dynamically modify the neutrino angular distributions.

It should be noted that the neutrino interaction rate in matter is dominated by the neutrino-nucleon cross-section, and the ratio  $\lambda_{\nu_e}/\lambda_{\bar{\nu}_e}$  cannot be changed significantly by the neutrino conversions on a global scale. In the deep interior of a SN, the effective average energy of  $\nu_e$  is larger than that of  $\bar{\nu}_e$  due to the non-null chemical potential. This contributes to a larger  $\nu_e$  interaction rate. Neutrino conversions could in principle reduce the average energy of  $\nu_e$  and bring it closer the one of  $\bar{\nu}_e$ .

We take the inputs of the SN snapshot at  $t_{p,b.} = 0.25$  s used in Sec. 3.2 as benchmark case. This case did not exhibit ELN crossings in the absence of pre-existing flavor conversions. We then impose that at a certain radius  $r_*$  flavor conversions are triggered possibly leading to flavor decoherence; the latter is one of the most extreme scenarios that one could expect. This effect can be mimicked by assuming that  $\lambda_{\nu_e}/\lambda_{\bar{\nu}_e} \rightarrow 1$  for  $r \geq r_*$ . We then change  $r_*$  in order to test whether the radius of the onset of flavor conversions would affect the ELN crossing development. In none of the studied cases, we find a significant modification of the ELN evolution and ELN crossings do not develop.

Although a more thorough analysis of the problem is required, we suspect that the non-locality of the conditions required for an ELN crossing is responsible for making the dynamical generation of ELN crossings unfeasible in a geometry that is spherically symmetric.

## 5. DISCUSSION AND CONCLUSIONS

The development of crossings between the angular distributions of  $\nu_e$  and  $\bar{\nu}_e$  (ELN crossings) is of relevance because it can possibly lead to fast pairwise conversions of neutrinos deep in the SN core with major consequences on the SN physics. It is vital to gain a qualitative understanding of this phenomenon. In this paper, using a simple yet insightful technique, we have qualitatively addressed this question focusing on the microphysics of neutrino-matter collisions in the SN core.

The highly non-linear nature of the neutrino flavor evolution along with the feedback on the flavor dynamics coming from neutrino-matter collisions makes a general self-consistent analysis impossible within current means. However, we have aimed to provide a rule of thumb for the occurrence of ELN crossings. To that purpose, we have constructed a simplified stationary and spherically symmetric SN model that takes into account the physics of collisions through an iterative approach, but neglects any asymmetry and further complications coming from the SN hydrodynamical instabilities. It should be noted that our assumption of spherical symmetry may be substantially broken either due to SN hydrodynamics (Tamborra et al. 2014b; Janka et al. 2016), or because the nature of the neutrino flavor evolution (Duan & Shalgar 2015; Mirizzi et al. 2015; Abbar et al. 2015).

We have shown that the conditions affecting the development of ELN crossings are not local in nature. In particular, the appearance of ELN crossings is determined by the slope of the baryon density profile together with the requirement that the  $\nu_e$  and  $\bar{\nu}_e$  number densities are comparable in the proximity of the decoupling region. Our simple spherically symmetric SN model hints that ELN crossings can only occur in the late stages of the accretion phase and in the cooling phase, under the assumption that a stationary configuration is reached. In fact, at earlier post-bounce times, a large excess of the  $\nu_e$  number density over the  $\bar{\nu}_e$  one prevents ELN crossings from occurring. The latter effect is determined by a baryon density profile that slowly varies with the radius, disfavoring the  $\nu_e$  and  $\bar{\nu}_e$  distributions from becoming similar. However, in the late accretion phase and cooling phase the distributions of  $\nu_e$  and  $\bar{\nu}_e$  naturally become more similar to each other,  $\nu_e$  and  $\bar{\nu}_e$  decouple in closer spatial regions, and favorable conditions for ELN crossings arise.

Due to the numerical challenges involved in solving the equations of motion that include neutrino-neutrino interactions, most of the focus has been on the linear stability analysis of the conditions under which instabilities in the flavor space can occur. However, if flavor instabilities are triggered in a small localized region of space, is it not clear if and under which conditions the flavor instability would spread, see e.g. Capozzi et al. (2017); Yi et al. (2019). One aspect of the question is whether the flavor evolution changes the neutrino interaction rates therefore leading to a dynamical generation of ELN crossings. Our stationary and spherically symmetric SN model suggests that ELN crossings cannot be generated dynamically, unless favorable conditions already exists in the SN core.

Our model neglects perturbations coming from global

asymmetries induced by the hydrodynamic instabilities occurring in SNe. However, it still provides good insights on the generation of ELN crossings under stationary conditions.

A concrete list of necessary and sufficient conditions under which fast pairwise conversions of neutrinos can occur in the SN core still remains unsettled. Our work provides new insights on the solution of this intriguing jigsaw.

We acknowledge insightful discussions with Thomas Janka, Georg Raffelt and Anna Suliga, and are grateful to Robert Bollig for granting access to the data of the  $18.6M_\odot$  SN model adopted in this work. SS and IT acknowledge support from the Villum Foundation (Project No. 13164). The work of IT has also been supported by the Knud Højgaard Foundation and the Deutsche Forschungsgemeinschaft through Sonderforschungsbereich SFB 1258 “Neutrinos and Dark Matter in Astro- and Particle Physics (NDM).

## REFERENCES

- Abbar, S., Duan, H., & Shalgar, S. 2015, *Phys. Rev.*, D92, 065019  
 Abbar, S., Duan, H., Sumiyoshi, K., Takiwaki, T., & Volpe, M. C. 2018  
 Abbar, S. & Volpe, M. C. 2019, *Phys. Lett.*, B790, 545  
 Azari, M. D., Yamada, S., Morinaga, T., Iwakami, W., Nagakura, H., & Sumiyoshi, K. 2019  
 Blaschke, D. N. & Cirigliano, V. 2016, *Phys. Rev.*, D94, 033009  
 Bowers, R. L. & Wilson, J. R. 1982, *ApJS*, 50, 115  
 Bruenn, S. W. 1985, *Astrophys. J. Suppl.*, 58, 771  
 Capozzi, F., Dasgupta, B., Lisi, E., Marrone, A., & Mirizzi, A. 2017, *Phys. Rev.*, D96, 043016  
 Capozzi, F., Dasgupta, B., & Mirizzi, A. 2018, *Phys. Rev.*, D98, 063013  
 Capozzi, F., Dasgupta, B., Mirizzi, A., Sen, M., & Sigl, G. 2019, *Phys. Rev. Lett.*, 122, 091101  
 Cirigliano, V., Paris, M. W., & Shalgar, S. 2017, *Phys. Lett.*, B774, 258  
 Dasgupta, B., Mirizzi, A., & Sen, M. 2017, *JCAP*, 1702, 019  
 Dasgupta, B., O’Connor, E. P., & Ott, C. D. 2012, *Phys. Rev.*, D85, 065008  
 Duan, H. & Shalgar, S. 2015, *Phys. Lett.*, B747, 139  
 Garching Supernova Archive, <https://www.mpa.mpg-garching.de/ccsnarchive/index.html>  
 Glas, R., Janka, H.-T., Melson, T., Stockinger, G., & Just, O. 2018  
 Izaguirre, I., Raffelt, G. G., & Tamborra, I. 2017, *Phys. Rev. Lett.*, 118, 021101  
 Janka, H.-T. 2012, *Ann. Rev. Nucl. Part. Sci.*, 62, 407  
 —. 2017  
 Janka, H.-T., Melson, T., & Summa, A. 2016, *Ann. Rev. Nucl. Part. Sci.*, 66, 341  
 Mirizzi, A., Mangano, G., & Saviano, N. 2015, *Phys. Rev.*, D92, 021702  
 Mirizzi, A., Tamborra, I., Janka, H.-T., Saviano, N., Scholberg, K., Bollig, R., Hüdepohl, L., & Chakraborty, S. 2016, *Riv. Nuovo Cim.*, 39, 1  
 Nagakura, H., Iwakami, W., Furusawa, S., Okawa, H., Harada, A., Sumiyoshi, K., Yamada, S., Matsufuru, H., & Imakura, A. 2018, *Astrophys. J.*, 854, 136  
 O’Connor, E. P. & Couch, S. M. 2018, *Astrophys. J.*, 865, 81  
 Ott, C. D., Burrows, A., Dessart, L., & Livne, E. 2008, *Astrophys. J.*, 685, 1069  
 Raffelt, G. G. 1996, *Stars as laboratories for fundamental physics*  
 Raffelt, G. G., Sarikas, S., & de Sousa Seixas, D. 2013, *Phys. Rev. Lett.*, 111, 091101, [Erratum: *Phys. Rev. Lett.* 113, no. 23, 239903 (2014)]  
 Richers, S. A., McLaughlin, G. C., Kneller, J. P., & Vlasenko, A. 2019  
 Sarikas, S., Tamborra, I., Raffelt, G. G., Hüdepohl, L., & Janka, H.-T. 2012, *Phys. Rev.*, D85, 113007  
 Sawyer, R. F. 2009, *Phys. Rev.*, D79, 105003  
 —. 2016, *Phys. Rev. Lett.*, 116, 081101  
 Sigl, G. & Raffelt, G. G. 1993, *Nucl. Phys.*, B406, 423  
 Stirner, T., Sigl, G., & Raffelt, G. G. 2018, *JCAP*, 1805, 016  
 Sumiyoshi, K., Takiwaki, T., Matsufuru, H., & Yamada, S. 2015, *Astrophys. J. Suppl.*, 216, 5  
 Tamborra, I., Hanke, F., Janka, H.-T., Müller, B., Raffelt, G. G., & Marek, A. 2014a, *Astrophys. J.*, 792, 96  
 Tamborra, I., Hüdepohl, L., Raffelt, G. G., & Janka, H.-T. 2017, *Astrophys. J.*, 839, 132  
 Tamborra, I., Raffelt, G. G., Hanke, F., Janka, H.-T., & Müller, B. 2014b, *Phys. Rev.*, D90, 045032

Vartanyan, D., Burrows, A., Radice, D., Skinner, A. M., & Dolence, J. 2019, Mon. Not. Roy. Astron. Soc., 482, 351  
Vlasenko, A., Fuller, G. M., & Cirigliano, V. 2014, Phys. Rev., D89, 105004  
Volpe, C., Vaananen, D., & Espinoza, C. 2013, Phys. Rev., D87, 113010  
Walk, L., Tamborra, I., Janka, H.-T., & Summa, A. 2019

Wu, M.-R. & Tamborra, I. 2017, Phys. Rev., D95, 103007  
Wu, M.-R., Tamborra, I., Just, O., & Janka, H.-T. 2017, Phys. Rev., D96, 123015  
Yi, C., Ma, L., Martin, J. D., & Duan, H. 2019, Phys. Rev., D99, 063005